An Evaluation for Iron Contamination in Silicon Solar Cell Using Ideality Factor and Machine Learning

Oleg Olikh, Oleg Lozitsky, and Oleksii Zavhorodnii

***Abstract*—The abstract goes here.**

***Index Terms*—ideality factor, silicon, n^+–p–p^+ structure, SCAPS, iron contamination, machine learning**

I. Introduction

NON–DESTRUCTIVE methods of evaluation of the impurities contamination in semiconductor crystals and structures, in particular solar cells (SCs), are important from an applied point of view. To date, a not little collection of direct methods (an infrared tomography, an electron-paramagnetic resonance, a non-stationary spectroscopy, etc.) as well as indirect methods (a surface photovoltage, a minority carrier lifetime measurements) has been developed to solve this problem. But almost all of them require special sample preparing or/and specialized equipment. At the same time, the current–voltage curve (IVC) measurement is a widespread method of SC characterization and allows to determine a number of fundamental SC parameters. Evidently SC parameters in particular and the processes of carrier propagation in general depend on electrically active defects presence; therefore there is a possibility in principle to determine the impurity concentration by IVC shape. And recent papers demonstrate a novel approach to extract defect properties from inexpensive IV measurements of completed devices [1].

One of the main obstacles of such a convenient and express method developing is the multiparameter relationship between the contamination of recombination centers and IVC's characteristics, which determined from experimental data. However, in the last decade, the deep learning, which are enable to solve problems without clear algorithmization, have been successfully used in various fields of theoretical and applied physics [2]–[4]. Furthermore, some authors have state that materials informatics (combination of material property calculations/measurements and informatics algorithms) was become the fourth (along with theory, simulations, and experiments) paradigm of science in the past few years [5]. This gives hope for an real implementation of aforesaid SC characterization method with using of deep learning approach (so to say "deep learning for deep levels").

In this work, we use numerical device models to show the possibility of such an approach fulfillment using the example of evaluation the iron concentration in n^+–p–p^+-Si by the ideality factor value. The reasons for aforesaid system consideration are following. Although the ideality factor $n = 2$ is often used to describe the trap related recombination, n value is known to depend on defect parameters, including the concentration [6]–[10]. Consequently the ideality factor is often used to characterize the various semiconductor barrier structures [10]–[15]. We have previously demonstrated [16] the correlation between defect contamination and n value, but the corresponding analytic expressions were not obvious and calibration curves were needed. The iron is a major contaminant as well as one of the most detrimental (and hence, best characterized) metal impurities in silicon photovoltaic devices [1], [17]. A simple back surface field (BSF) n^+–p–p^+ structure is important from an applied point of view.

The deep learning is based on learn by examples. In this work the labeled dataset has been simulated by using SCAPS-1D [18], [19], which was widely used to model silicon-based devices [20]–[22] as well. Obviously, experimental measurements would be preferable, but it is practically impossible to find the necessary thousands of samples with the required parameters.

The work milestone are following (i) the IVC simulation of numerous n^+–p–p^+-Si structure with various parameters for different temperatures; (ii) the fitting of the IVC set according to the two–diode model and the extraction of n value set; (iii) the training of deep neural network (DNN) to estimate an iron–related defect contamination by using SC's base thickness as well as doping level, temperature and ideality factor value; (iv) the DNN testing. Fig. 1 shows a schematic of machine learning based approaches to iron contamination evaluation in which the simulation provides training data. The consequent Sections give the details.

II. Simulation Details

A. Temperature Dependencies of Material Parameters

To receive more relevant labeled data, the IVC simulation was performed with regard to following silicon properties:

1) the bandgap temperature dependence according to Pässler equation [23];
2) the doping induced bandgap narrowing [24];
3) the thermal carrier velocities from [25];
4) the temperature dependence of effective states density according to [26];
5) the free carrier effective masses from [27]

The authors are with the Faculty of Physics, Taras Shevchenko National University of Kyiv, 64/13, Volodymyrska Street, City of Kyiv, Ukraine, 01601 (e-mail: olegolikh@knu.ua).

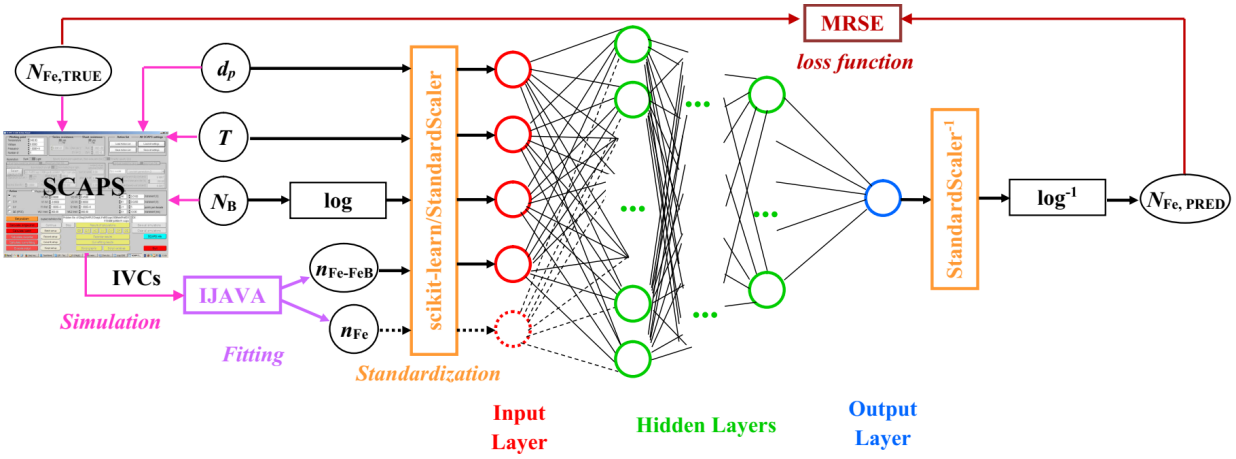

Fig. 1. Flowchart of the work steps. Additional details are discussed in the body of the article.

6) the carrier mobilities according to Klaassen's theory [28];
7) the temperature and doping level dependencies of band–to–band and Auger recombination coefficients from [29] and [30] respectively.

B. Defect Parameters

The simulation was carried out under the assumption that the defect–assisted recombination was bound up with iron–related deep levels. We have assumed uniform iron atom distribution in both SC base (p–region) and BSF–layer (p^+–region) with concentration N_{Fe}. Simulations were carried out for two cases. In the first equilibrium one, the iron is believed to be both in the interstitial lattice position (Fe_i) and in the trigonal pair with shallow acceptors (boron, $\mathrm{Fe}_i\mathrm{B}_s$). The pair's fraction does not constant in SC regions and is given by [31], [32]

$$\frac{N_{\mathrm{FeB}}}{N_{\mathrm{Fe}}} = \frac{N_{\mathrm{B}} 10^{-23} \exp\left(-\frac{E_b}{kT}\right)}{\left[1+\frac{N_{\mathrm{B}}}{10^{23}}\exp\left(-\frac{E_b}{kT}\right)\right]\left[1+\exp\left(-\frac{F-E_{\mathrm{Fe}_i}}{kT}\right)\right]}, \quad (1)$$

where N_{B} is the boron concentration, F is the Fermi level, $E_b = 0.582$ eV is the binding energy of the $\mathrm{Fe}_i\mathrm{B}_s$ pairs, E_{Fe_i} is the donor level, associated with Fe_i. This case referred as "Fe-FeB" hereafter.

In the second one (referred as "Fe"–case), the Fe_i was suggested to be only present with uniform distribution. Such state can be realized by heat treatment (210°C, 3 min) [33] or intense illumination [34].

The donor level $E_{\mathrm{Fe}_i} = E_V + 0.394$ eV with electron $\sigma_{n,\mathrm{Fe}} = 3.47\times10^{-11}T^{-1.48}$ cm^2 and hole $\sigma_{p,\mathrm{Fe}} = 4.54\times10^{-16}\exp\left(-\frac{0.05}{kT}\right)$ cm^2 capture cross-sections [31], [35] was associated with Fe_i. The donor level $E^{\mathrm{D}}_{\mathrm{FeB}} = E_V + 0.10$ eV, $\sigma^{\mathrm{D}}_{n,\mathrm{FeB}} = 4\times10^{-13}$ cm^2, $\sigma^{\mathrm{D}}_{p,\mathrm{FeB}} = 2\times10^{-14}$ cm^2 and acceptor level $E^{\mathrm{A}}_{\mathrm{FeB}} = E_C - 0.26$ eV, $\sigma^{\mathrm{A}}_{n,\mathrm{FeB}} = 5.1\times10^{-9}T^{-2.5}$ cm^2, $\sigma^{\mathrm{A}}_{p,\mathrm{FeB}} = 3.32\times10^{-10}\exp\left(-\frac{0.262}{kT}\right)$ cm^2 [31], [35], [36] were used in simulation for $\mathrm{Fe}_i\mathrm{B}_s$.

C. Structure Parameters

The dark IVCs for n^+–p–p^+-Si structure were simulated. The thickness and donor concentration for emitter layer (n^+) were 0.5 μm and 10^{19} cm^{-3}. The BSF–layer with thickness 1 μm and acceptor concentration 5×10^{18} cm^{-3} was used. The base thickness d_p (150–240 μm) and doping level (boron concentration, $N_{\mathrm{B}} = 10^{15}$–10^{17} cm^{-3}) changed from one simulation to another. Other varied parameters were temperature ($T = 290$–340 K) and iron concentration ($N_{\mathrm{Fe}} = 10^{10}$–$10^{13}$ cm^{-3}).

4 d_p values, 9 N_{B} values, 11 T values and 19 N_{Fe} values, which evenly (for T and d_p in linear scale, for N_{Fe} and N_{B} in logarithmic scale) distributed over the above ranges, formed a kind of parameter's grid. To obtain training dataset, 15048 IVCs were simulated in Fe-case and Fe-FeB-case for nodes of grid.

Besides IVCs were prepared for several test datasets as well. For example, one IVCs set was simulated by using d_p, N_{Fe} and N_{B} values from grid nodes and divergent T values. The corresponding test dataset is labeled "T-varied" from now on. The value of d_p, N_{Fe} and N_{B} are divergent from grig in "d-varied", "Fe-varied" and "B-varied" dataset, respectively. "All-varied" dataset was calculated with using all parameter values, unmatched to ones of training dataset. The precise parameters values are listed in Supplementary Material.

D. Ideality factor determination

The simulated IVCs were fitted by using double diode model [37] equation with neglecting of both series and shunt resistances:

$$I = I_{01}\left[\exp\left(-\frac{qV}{kT}\right)-1\right] + I_{02}\left[\exp\left(-\frac{qV}{nkT}\right)-1\right], \quad (2)$$

where I_{01} and I_{02} are the saturation currents. The fitting was done by using the meta–heuristic method IJAVA [38].

The ideality factor value n_{Fe} and $n_{\mathrm{Fe-FeB}}$ corresponds to Fe-case and Fe-FeB-case respectively. The typical simulated dependencies of the ideality factor are shown in Fig. 2. It should be noted that n can takes equal values for different

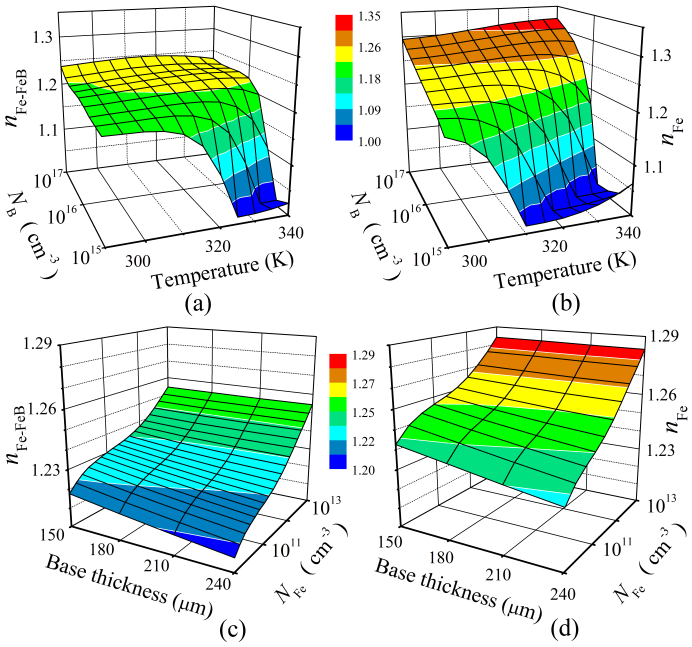

Fig. 2. Ideality factor as a function of the temperature and boron concentration (a, b) or the base thickness and iron concentration (c,d). The cases of Fe_iB_s and Fe_i coexistence (a, c) and interstitial iron presence only (b, d). $N_{Fe} = 10^{10}$ cm^{-3} (a,b), $d_p = 180$ μm (a, b), $N_B = 10^{16}$ cm^{-3} (c, d), $T = 320$ K (c, d).

parameters values and dependencies of n_{Fe} and n_{Fe-FeB} are slightly vary. The discussion about n_{Fe} and n_{Fe-FeB} values are presented elsewhere [39].

III. Results of Deep Neural Network Using

We have tried to construct the DNN, which is able to estimate iron contamination by using SC parameters (d_p and N_B) and results of IVC fitting (ideality factor value) taking into account the measurement temperature. In one case, the result of only one dark IV measurement was used and the set of DNN input parameters (one DNN–sample) consisted of $\{d_p, N_B, T, n_{Fe-FeB}\}$. Such case can be easy realized in practice and corresponding neural network referred as n_{Fe-FeB} DNN hereafter. In another case the set $\{d_p, N_B, T, n_{Fe-FeB}, n_{Fe}\}$ was used in DNN input. In practice terms, the obtaining of such a set requires additional SC processing (e.g. intense illumination) and two IV measuring. The label n_{Fe-FeB}–n_{Fe} DNN is used below.

The DNN's flowchart is shown on Fig. 1. The Keras API [40] was used to set up DNN with dense layers. Four hidden layers with 300, 100, 30 and 30 nodes were selected. The activation function was chosen to be Relu. The learning rate, batch size and number of epochs were kept at 0.01, 8 and 1000 respectively. $\log N_B$ and $\log N_{Fe}$ were used instead N_B and N_{Fe} in DNN training and testing. Standardization of a dataset was done by using *StandardScaler* from *scikit-learn* (mean $= 0$, standard deviation $= 1$). The loss function was chosen mean square relative error (MSRE):

$$\mathrm{MSRE} = \frac{1}{N_s}\sum_{i=1}^{N_s}\frac{(N_{\mathrm{Fe,TRUE,i}} - N_{\mathrm{Fe,PRED,i}})^2}{N_{\mathrm{Fe,TRUE,i}}\cdot N_{\mathrm{Fe,PRED,i}}}, \qquad (3)$$

TABLE I
Results of 10–Fold Cross–Validation

Dataset	MSRE	
	n_{Fe-FeB} DNN	n_{Fe-FeB}–n_{Fe} DNN
training	0.29 ± 0.07	0.09 ± 0.04
full	0.30 ± 0.08	0.05 ± 0.02

TABLE II
A Mean Square Relative Error Of DNNs on Test Dataset

Dataset	n_{Fe-FeB} DNN	n_{Fe-FeB}–n_{Fe} DNN
T–varied	0.46	0.06
B–varied	1.2	0.25
d–varied	0.36	0.06
Fe–varied	0.06	0.03
All–varied	0.49	0.10

where N_s is the number of samples in dataset, $N_{\mathrm{Fe,TRUE,i}}$ is the iron concentration, which used for simulation of i–th sample, $N_{\mathrm{Fe,PRED,i}}$ is the DNN prediction for i–th sample.

10–fold cross–validation was used to estimate DNN training. The results are listed in Table I. One can see that n_{Fe-FeB}–n_{Fe} DNN shows much better results.

DNNs, trained by parameters grid nodes data, were applied to test datasets. Results are presented in Fig. 3 (a)-(e), (g)-(k) and in Table II. As it is shown, the n_{Fe-FeB} DNN can be quite wrong for some samples ($\{d_p, N_B, T, n_{Fe-FeB}\}$ sets). The largest errors are observed for doping level values, which unused during network learning (B-varied dataset, Fig. 3(c)). On the other hand, the variation in N_{Fe} value are well detected even n_{Fe-FeB} DNN: $\mathrm{MSRE} = 0.06$ only and SRE does not exceed 0.01 for 90% of samples (see lines in Fig. 3(d)).

The one-parameters divergence in other cases from training magnitude has not vital importance: the $N_{\mathrm{Fe,TRUE}}$ and $N_{\mathrm{Fe,PRED}}$ difference can be occasionally significant, but SRE for about 80 percent of the samples does not exceed 0.01 in cases of T-varied and d-varied dataset — see Fig. 3(a),(b). At the same time, the predictive power of the n_{Fe-FeB} DNN is very limited in the All-varied dataset: the SRE is less than 0.1 in 30 percent of cases only.

It is obviously, that n_{Fe-FeB} DNN properties can can be improved by a configuration tuning as well as an extension in training dataset. But in our opinion, the network predictive ability is fundamentally limited by n_{Fe-FeB} vs N_{Fe} dependence ambiguity (see details elsewhere [39]). The increase in the input parameter number is quite expected to enhances the DNN capability. But the expected improvement of the of n_{Fe-FeB}–n_{Fe} DNN must be also caused by the removal of a certain degeneration of correlation between an ideality factor value and an iron concentration (a kind of splitting).

Indeed, one can see the improvement in operating characteristic of n_{Fe-FeB}–n_{Fe} DNN in comparison with n_{Fe-FeB} DNN. The improvement manifests itself both in the MSRE decrease (see Table II) and in the almost complete absence of huge difference in $N_{\mathrm{Fe,TRUE}}$ and $N_{\mathrm{Fe,PRED}}$ values. Really, the maximum SRE does not exceed 1 and SRE is less than 0.1 for 60% of samples even for the All-varied test dataset —

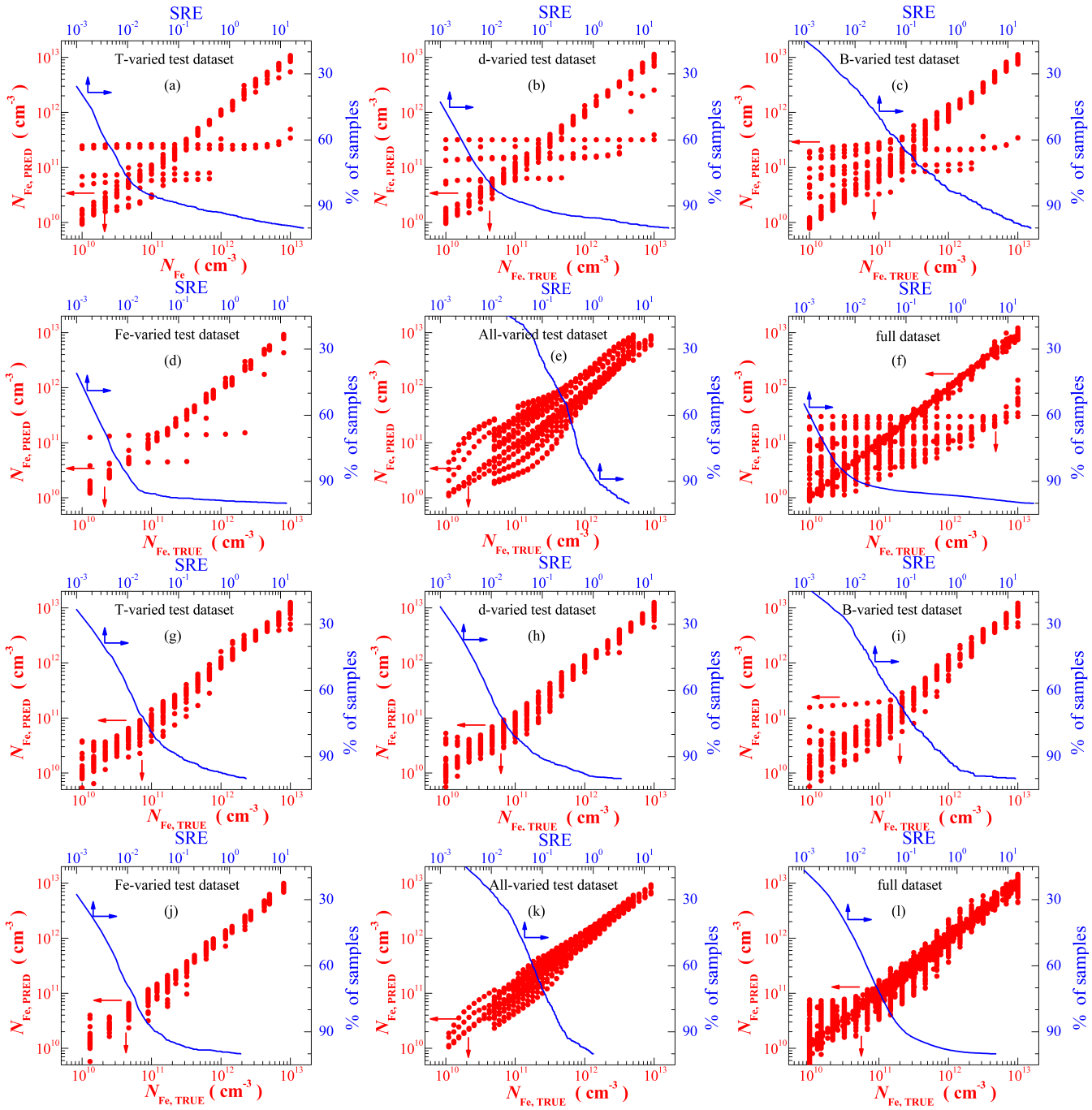

Fig. 3. Comparison of iron contamination retrieval results (red points) and part of samples with SRE not exceeding a certain value (blue lines). $n_{\mathrm{Fe-FeB}}$ DNN and $n_{\mathrm{Fe-FeB}}$–n_{Fe} DNN were used in panels (a)–(f) and (g)–(l), respectively. Test dataset: T-varied (a, g), d-varied (b, h), B-varied (c, i), Fe-varied (d, j), All-varied (e, k). DNNs were trained by training dataset ((a)–(e), (g)–(k)) or full (f, l) dataset.

see Fig. 3(k).

Despite the difference in predicting accuracy, the $n_{\mathrm{Fe-FeB}}$–n_{Fe} DNN's features are similar to $n_{\mathrm{Fe-FeB}}$ DNN's ones. Thus difference in N_{B} value from training dataset is the most troublesome case (Fig. 3(i)). The enjoyable (from a practical point of view) attribute is an ability to predict iron concentration value, which not used under learning.

It is known [40] that the increase of labeled dataset to train on leads to improve deep neural network results. We have used all simulated data (so-called full dataset) to train both $n_{\mathrm{Fe-FeB}}$–n_{Fe} DNN and $n_{\mathrm{Fe-FeB}}$ DNN as well. The results are presented in Table I and Fig. 3 (f) and (l). Surprisingly the expansion of training base did not make better the results of cross–validation for $n_{\mathrm{Fe-FeB}}$ DNN. In our opinion, the mentioned above features of $n_{\mathrm{Fe-FeB}}$ vs N_{Fe} dependence are a reason of such result. At the same time the increase in number of samples leds to essential raise trainability of network, which uses two ideality factor value.

The results on IVC simulation, n_{Fe} and $n_{\mathrm{Fe-FeB}}$ values and trained DNNs are presented at

https://github.com/olegolikh/IVcharacteristics.git.

IV. Conclusion

The conclusion goes here.

Acknowledgment

The work was supported by National Research Foundation of Ukraine by the state budget finance (project 2020.02/0036 "Development of physical base of both acoustically controlled modification and machine learning–oriented characterization for silicon solar cells")

References

[1] R. C. Kurchin, J. R. Poindexter, V. Vähänissi, H. Savin, C. del Cañizo, and T. Buonassisi, "How much physics is in a current–voltage curve? inferring defect properties from photovoltaic device measurements," *IEEE J. Photovolt.*, vol. 10, no. 6, pp. 1532–1537, Nov 2020.

[2] G. Carleo, I. Cirac, K. Cranmer, L. Daudet, M. Schuld, N. Tishby, L. Vogt-Maranto, and L. Zdeborová, "Machine learning and the physical sciences," *Rev. Mod. Phys.*, vol. 91, p. 045002, Dec 2019.

[3] S. Ju, S. Shimizu, and J. Shiomi, "Designing thermal functional materials by coupling thermal transport calculations and machine learning," *J. Appl. Phys.*, vol. 128, no. 16, p. 161102, Oct 2020.

[4] S. Rodrigues, H. G. Ramos, and F. Morgado-Dias, "Machine learning pv system performance analyser," *Prog. Photovoltaics Res. Appl.*, vol. 26, no. 8, pp. 675–687, Aug 2018.

[5] S. Ju, S. Shimizu, and J. Shiomi, "Designing thermal functional materials by coupling thermal transport calculations and machine learning," *J. Appl. Phys.*, vol. 128, no. 16, p. 161102, Oct 2020.

[6] J. Beier and B. Voss, "Humps in dark I–V–curves–analysis and explanation," in *Conference Record of the Twenty Third IEEE Photovoltaic Specialists Conference - 1993 (Cat. No.93CH3283-9)*, May 1993, pp. 321–326.

[7] K. McIntosh, P. Altermatt, and G. Heiser, "Depletion–region recombination in silicon solar cells. when does $mdr = 2$?" in *16th European Photovoltaic Solar Energy Conference: Proceedings of the International Conference and Exhibition*. Publisher:James and James (Science Publishers) Ltd, 2000, pp. 250–253.

[8] A. Kaminski, J. J. Marchand, H. El Omari, A. Laugier, Q. N. Le, and D. Sarti, "Conduction processes in silicon solar cells," in *Conference Record of the Twenty Fifth IEEE Photovoltaic Specialists Conference – 1996*, May 1996, pp. 573–576.

[9] Z. Hameiri, K. McIntosh, and G. Xu, "Evaluation of recombination processes using the local ideality factor of carrier lifetime measurements," *Sol. Energy Mater. Sol. Cells*, vol. 117, pp. 251–258, Oct 2013.

[10] A. S. H. van der Heide, A. Schonecker, J. H. Bultman, and W. C. Sinke, "Explanation of high solar cell diode factors by nonuniform contact resistance," *Progress in Photovoltaics: Research and Applications*, vol. 13, no. 1, pp. 3–16, Jan 2005.

[11] L. Duan, H. Yi, C. Xu, M. B. Upama, M. A. Mahmud, D. Wang, F. H. Shabab, and A. Uddin, "Relationship between the diode ideality factor and the carrier recombination resistance in organic solar cells," *IEEE Journal of Photovoltaics*, vol. 8, no. 6, pp. 1701–1709, Nov 2018.

[12] J. Chen, M. Zhu, X. Lu, and X. Zou, "Electrical characterization of gan schottky barrier diode at cryogenic temperatures," *Appl. Phys. Lett.*, vol. 116, no. 6, p. 062102, Feb 2020.

[13] P. Dalapati, N. Manik, and A. Basu, "Analysis of the temperature dependence of diode ideality factor in InGaN-based UV-A light-emitting diode," *Semiconductors*, vol. 54, no. 10, pp. 1284–1289, Oct 2020.

[14] P. Calado, D. Burkitt, J. Yao, J. Troughton, T. M. Watson, M. J. Carnie, A. M. Telford, B. C. O'Regan, J. Nelson, and P. R. Barnes, "Identifying dominant recombination mechanisms in perovskite solar cells by measuring the transient ideality factor," *Phys. Rev. Applied*, vol. 11, p. 044005, Apr 2019.

[15] S. V. Bulyarskiy, A. V. Lakalin, M. A. Saurov, and G. G. Gusarov, "The effect of vacancy-impurity complexes in silicon on the current–voltage characteristics of p–n junctions," *J. Appl. Phys.*, vol. 128, no. 15, p. 155702, Oct 2020.

[16] O. Olikh, "Relationship between the ideality factor and the iron concentration in silicon solar cells," *Superlattices Microstruct.*, vol. 136, p. 106309, Dec 2019.

[17] J. Schmidt, "Effect of dissociation of iron–boron pairs in crystalline silicon on solar cell properties," *Progress in Photovoltaics: Research and Applications*, vol. 13, no. 4, pp. 325–331, Jun 2005.

[18] M. Burgelman, P. Nollet, and S. Degrave, "Modelling polycrystalline semiconductor solar cells," *Thin Solid Films*, vol. 361–362, pp. 527–532, Feb 2000.

[19] K. Decock, S. Khelifi, and M. Burgelman, "Modelling multivalent defects in thin film solar cells," *Thin Solid Films*, vol. 519, no. 21, pp. 7481–7484, Aug 2011.

[20] E. Hu, G. Yue, R. Zhang, Y. Zheng, L. Chen, and S. Wang, "Numerical simulations of multilevel impurity photovoltaic effect in the sulfur doped crystalline silicon," *Renewable Energy*, vol. 77, pp. 442–446, May 2015.

[21] A. Hamache, N. Sengouga, A. Meftah, and M. Henini, "Modeling the effect of 1 MeV electron irradiation on the performance of n^+–p–p^+ silicon space solar cells," *Radiat. Phys. Chem.*, vol. 123, pp. 103–108, Jun 2016.

[22] K. Kim, J. Gwak, S. K. Ahn, Y.-J. Eo, J. H. Park, J.-S. Cho, M. G. Kang, H.-E. Song, and J. H. Yun, "Simulations of chalcopyrite/c-si tandem cells using scaps-1d," *Sol. Energy*, vol. 145, pp. 52–58, 2017.

[23] R. Pässler, "Dispersion-related description of temperature dependencies of band gaps in semiconductors," *Phys. Rev. B*, vol. 66, p. 085201, Aug 2002.

[24] D. Yan and A. Cuevas, "Empirical determination of the energy band gap narrowing in p^+ silicon heavily doped with boron," *J. Appl. Phys.*, vol. 116, no. 19, p. 194505, Nov 2014.

[25] M. A. Green, "Intrinsic concentration, effective densities of states, and effective mass in silicon," *J. Appl. Phys.*, vol. 67, no. 6, pp. 2944–2954, Mar 1990.

[26] R. Couderc, M. Amara, and M. Lemiti, "Reassessment of the intrinsic carrier density temperature dependence in crystalline silicon," *J. Appl. Phys.*, vol. 115, no. 9, p. 093705, Mar 2014.

[27] W. O'Mara, R. Herring, and L. Hant, *Handbook of semiconductor silicon technology*. New Jersey, USA: Noyes Publications, 1990.

[28] D. Klaassen, "A unified mobility model for device simulation — I. model equations and concentration dependence," *Solid-State Electron.*, vol. 35, no. 7, pp. 953– 959, Jul 1992.

[29] H. T. Nguyen, S. C. Baker-Finch, and D. Macdonald, "Temperature dependence of the radiative recombination coefficient in crystalline silicon from spectral photoluminescence," *Appl. Phys. Lett.*, vol. 104, no. 11, p. 112105, Mar 2014.

[30] P. P. Altermatt, J. Schmidt, G. Heiser, and A. G. Aberle, "Assessment and parameterisation of Coulomb–enhanced Auger recombination coefficients in lowly injected crystalline silicon," *J. Appl. Phys.*, vol. 82, no. 10, pp. 4938–4944, Nov 1997.

[31] J. D. Murphy, K. Bothe, M. Olmo, V. V. Voronkov, and R. J. Falster, "The effect of oxide precipitates on minority carrier lifetime in p–type silicon," *J. Appl. Phys.*, vol. 110, no. 5, p. 053713, Sep 2011.

[32] W. Wijaranakula, "The reaction kinetics of iron–boron pair formation and dissociation in p–type silicon," *J. Electrochem. Soc.*, vol. 140, no. 1, pp. 275–281, Jan 1993.

[33] G. Zoth and W. Bergholz, "A fast, preperetion-free method to detect irpn in silicon," *J. Appl. Phys.*, vol. 67, no. 11, pp. 6764–6771, Jun 1990.

[34] L. J. Geerligs and D. Macdonald, "Dynamics of light-induced feb pair dissociation in crystalline silicon," *Appl. Phys. Lett.*, vol. 85, no. 22, pp. 5227–5229, Nov 2004.

[35] F. E. Rougieux, C. Sun, and D. Macdonald, "Determining the charge states and capture mechanisms of defects in silicon through accurate recombination analyses: A review," *Solar Energy Materials and Solar Cells*, vol. 187, pp. 263 – 272, Dec 2018.

[36] A. A. Istratov, H. Hieslmair, and E. Weber, "Iron and its complexes in silicon," *Applied Physics A: Materials Science & Processing*, vol. 69, no. 1, pp. 13–44, Jul 1999.

[37] O. Breitenstein, "Understanding the current-voltage characteristics of industrial crystalline silicon solar cells by considering inhomogeneous current distributions," *Opto–Electronics Review*, vol. 21, no. 3, pp. 259–282, Sep 2013.

[38] K. Yu, J. Liang, B. Qu, X. Chen, and H. Wang, "Parameters identification of photovoltaic models using an improved JAYA optimization algorithm," *Energy Conversion and Management*, vol. 150, pp. 742–753, Oct 2017.

[39] O. Y. Olikh and O. V. Zavhorodnii, "Modeling of ideality factor value in n^+–p–p^+–si structure," *Journal of Physical Studies*, vol. 24, no. 4, p. 4701, 2020.

[40] F. Chollet, *Deep Learning with Python*, 2nd ed. Manning, 2017.

Oleg Olikh was born in Kyiv, Ukraine, in 1974. He received the Ph.D. (2001) and D.Sc. (2018) in solid state physics from Taras Shevchenko National University of Kyiv. Since 2001, he has been an associate professor in the Department of General Physics at Taras Shevchenko National University of Kyiv. His research interests in semiconductor physics have focused on external (radiation, ultrasound) influence on properties of semiconductor devices.